Supplementary Information: Improved SABRE hyperpolarisation using pulse sequences to reduce effective coupling

Vitaly P. Kozinenko,[a] Bogdan A. Rodin,[a] James Eills,[b] Ilai Schwartz,[a] Stephan Knecht,[a] and Laurynas Dagys*[c]*

[a] *NVision Imaging Technologies GmbH, Wolfgang-Paul Straße 2, 89081 Ulm, Germany.*

[b] *Forschungszentrum Jülich,Wilhelm-Johnen-Straße,52428 Jülich, Germany*

[c] *Institute of Chemical Physics, Vilnius University, Saulėtekio av. 3, Vilnius LT10257, Lithuania.*

Correspondence: stephan@nvision-imaging.com; laurynas.dagys@ff.vu.lt*

1 EXPERIMENTAL SABRE OPTIMISATIONS

1.1 *Experimental setup*

This study involved a fully automated experimental setup (Fig. S1). Automation was achieved using a custom Python-based interface handling software and hardware triggers and communicating with multiple instruments. These include electronically controlled valves for the gas manifold, National Instruments analog signal generator, power supply for the bias field coil, motor driver for transportation of the sample as well as NMR spectrometer. Each instrument was triggered with <50 ms time accuracy while samples were transported between the magnetic shield and NMR magnet within 1.2 seconds. The low-field chamber consisted of TwinLeaf MS-1 shield and a saddle coil. This coil was connected to the Kemo audio amplifier and used for generating oscillating magnetic field. The bias magnetic field was produced by the built-in Helholtz coil of the magnetic shield powered by Rohde and Schwarz power supply. Two-way trigger protocol with the spectrometer allowed full synchronicity with the Python-based interface.

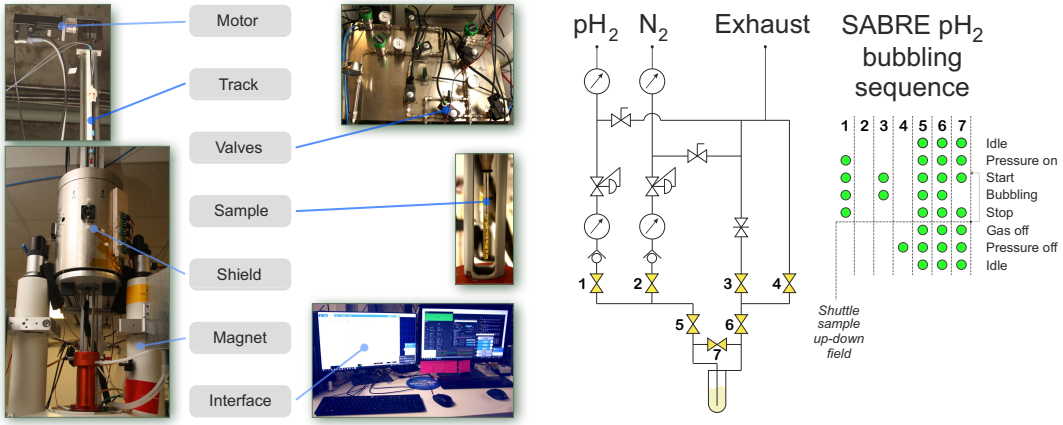

Figure S1. Left - photographs of the experimental setup used for the study. Right - the schematics of the automated valve system and their opening sequences during the SABRE experiments. Green dots indicate open state of a numbered valve. Other valves are mechanically regulated. The sample is transported from magnetic shield to the NMR magnet after the bubbling is stopped. Due to repeatable nature of SABRE experiments, multiple runs can be performed by transporting sample back to low-field chamber and starting the bubbling with parahydrogen again. SABRE pulse sequences are initiated during the state of bubbling and stopped together with the bubbling.

1.2 *SABRE-SHEATH*

SABRE-SHEATH was optimised by varying the static magnetic fields at which SABRE polarisation takes places. The example data is shown in Fig. S2 and the optimised values are given in the table below.

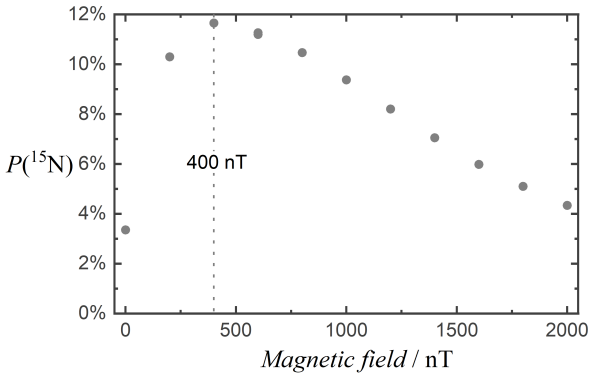

Figure S2. SABRE-SHEATH optimization of ^{15}N polarisation achieved on ^{15}N-acetonitrile at different bias fields during bubbling with parahydrogen. Experiments were performed at room temperature. Optimal SABRE-SHEATH field is indicated.

Table 1. Optimal **SABRE-SHEATH** bias fields and ^{15}N polarisation levels achieved at room temperature. Errors were estimated by performing experiments six times.

System	Optimal field	^{15}N polarisation
^{15}N-acetonitrile	400 nT	$11.7 \pm 0.4\%$
^{15}N-pyridine	400 nT	$6.8 \pm 0.2\%$
Metronidazole	800 nT	$9.1 \pm 0.6\%$

1.3 *SABRE-SLIC*

SABRE-SLIC was optimised by varying the amplitude of the oscillating magnetic field at a bias field of 98 μT. The frequency was set to the ^{15}N resonance frequency at this field. The example data is shown in Fig. S3 and the optimised values are given in the table below.

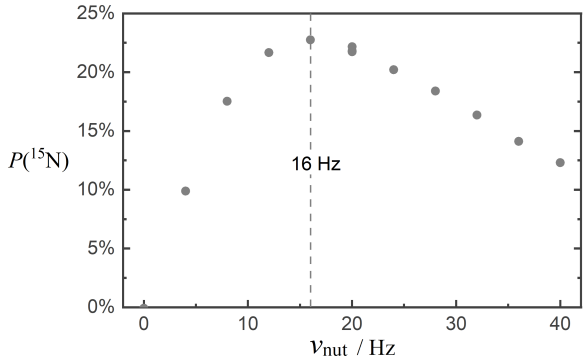

Figure S3. SABRE-SLIC optimisation of ^{15}N polarisation achieved on ^{15}N-acetonitrile at different oscillating field B_1 amplitudes with bias field set to 98 μT. Experiments were performed at room temperature. Optimal amplitude is indicated by the dashed line.

Table 2. Optimal **SABRE-SLIC** B_1 amplitudes and ^{15}N polarisation levels achieved at room temperature. Experiments were performed at fixed 98 μT bias field. Errors were estimated by repeating experiments four times.

System	B_1 amplitudes	^{15}N polarisation
^{15}N-acetonitrile	16 Hz	$21.1 \pm 0.3\%$
^{15}N-pyridine	16 Hz	$15.2 \pm 0.9\%$
Metronidazole	16 Hz	$12.9 \pm 0.2\%$

1.4 *SABRE-DRF-SLIC*

SABRE-DRF-SLIC experiments were performed by utilising two transverse oscillating fields. The first was set to be resonant with ^{1}H at amplitude of 80 Hz. The second field was set to amplitude of 16 Hz and with a slight mismatch with the ^{15}N Larmor frequency. The mismatch was varied as shown in Fig. S4. The optimal values together which the effective angle of the effective field for ^{15}N spins are indicated in the table below.

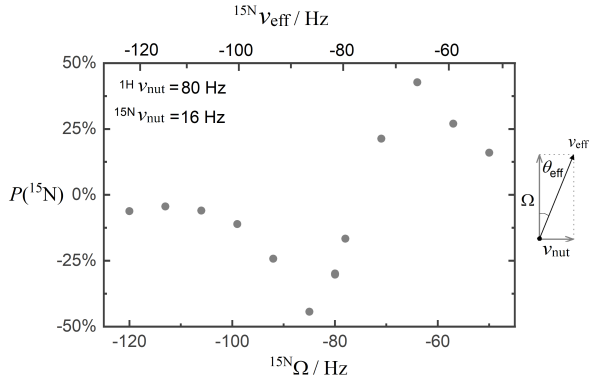

Figure S4. SABRE-DRF-SLIC optimization of ^{15}N polarisation achieved on ^{15}N-acetonitrile at different oscillating field frequency offsets. The bias magnetic field was set to 98 μT. Experiments were performed at room temperature. The effective angle is depicted on the right for clarity.

Table 3. Optimal **SABRE-DRF-SLIC** parameters and ^{15}N polarisation levels achieved at room temperature. Experiments were performed at fixed 96 μT bias field. Errors were estimated by repeating experiments four times. Number of cycles was adjusted for overall duration of 30 s.

System	$^{1H}\nu_{\text{nut}}$	$^{15N}\nu_{\text{nut}}$	$^{15N}\Omega$	θ_{eff}	^{15}N polarisation
^{15}N-acetonitrile	80 Hz	16 Hz	-64 Hz	14.0°	$45.3 \pm 0.3\%$
^{15}N-pyridine	80 Hz	16 Hz	-64 Hz	14.0°	$23.0 \pm 1.6\%$
Metronidazole	80 Hz	30 Hz	-104 Hz	16.1°	$3.7 \pm 0.1\%$

1.5 *SABRE-PulsePol*

SABRE-PulsePol experiments were performed by utilising a single channel sequence. The pulses were resonant with ^{15}N spins with amplitude of 600 Hz. The bias field was elevated to 1 mT to avoid Bloch-Siegert shift. The pulse shape was set to Gaussian with 10% truncation to avoid possible ^{1}H excitation. Experimental optimisation involved exploration of two parameter space, the phase φ and evolution time τ. The sequence is the depicted in the main text. An profile acquired by varying phase at fixed evolution time is shown in Fig. S5 and the optimised values are provided in the table below.

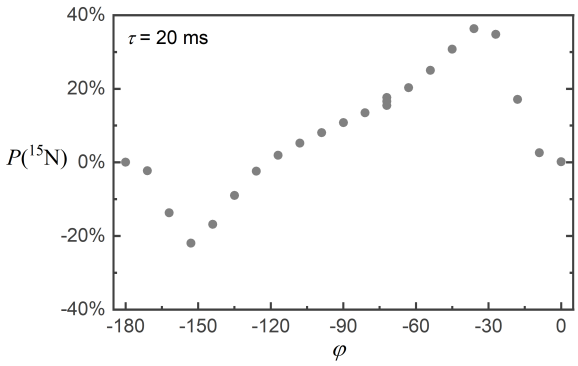

Figure S5. SABRE-PulsePol optimisation of ^{15}N polarisation achieved on ^{15}N-acetonitrile at different phase φ settings at fixed PulsePol cycle time τ. The bias magnetic field was set to 1000 μT.

Table 4. Optimal **SABRE-PulsePol** phase step and cycle times and ^{15}N polarisation levels achieved at room temperature. Experiments were performed at fixed 1 mT bias field. Errors were estimated by repeating experiments four times. Number of cycles was adjusted for overall duration of 30 s.

System	Phase step φ	Cycle time τ_{PP}	^{15}N polarisation
^{15}N-acetonitrile	-36°	20.0 ms	$48.6 \pm 0.3\%$
^{15}N-pyridine	-36°	22.2 ms	$29.4 \pm 1.6\%$
Metronidazole	-72°	16.0 ms	$4.5 \pm 0.5\%$

SABRE AT LOWER TEMPERATURE

We have also ran an additional experiments on metronidazole system at reduced temperature of 5°C and optimised each SABRE method as previously described. The results are summarized in Fig. S6. We have observed an overall increase in PulsePol and DRF-SLIC performance at lower temperature. However, the maximum ^{15}N polarisation was still acquired using SABRE-SLIC which suggests that the exchange rate may be expected to be relatively high which experimentally was determined to be around 60 s^{-1}.

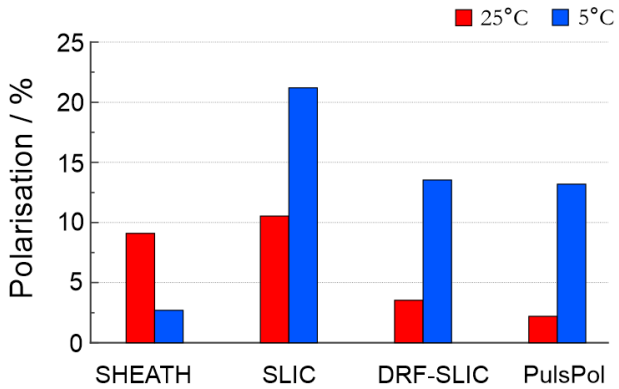

Figure S6. ^{15}N polarisation levels achieved on MTZ using different SABRE methods at 25°C and 5°C.

2 NUMERICAL CALCULATIONS

To perform the numerical simulations, the superoperator approach was used which allows for accounting of coherent, relaxation, and exchange dynamics. The exact theoretical details can be found elsewhere[1], and the exact implementation can be found in the repository link - 10.5281/zenodo.18927246. For the calculation simplicity, the rapid parahydrogen exchange is assumed. In this analysis, we considered a single ^{15}N nucleus in the substrate, while the SABRE complex yields a 3-spin system with two additional protons derived from parahydrogen. For the case of continuous wave methods, the steady-state solution was derived from the null-space. For pulsed methods (PulsePol), 50 seconds of evolution time was granted. The $J_{\mathrm{HH}} = -7.7$ Hz and the $J_{\mathrm{NH}} = -21$ Hz. Relaxation was phenomenological, with $T_1 = 6$ seconds on protons and 20 seconds on nitrogen.

2.1 *SHEATH*

The simulation results for SABRE-SHEATH are shown in Figure S7. In the slow-to-intermediate exchange regime, the optimal B_0 values lie between 200 and 600 nT. This coincides well with our experimental data, see Table 1, where all investigated compounds exhibited an optimal amplitude of 400 nT, with the exception of 800 nT for Metronidazole which has the largest k_{d}. Interestingly, the optimal B_0 experiences a sharp increase beyond $k_{\mathrm{d}} \approx 90$ s^{-1}. In this fast-exchange region, the system deviates from the standard Level Anti-Crossing (LAC) condition, effectively sacrificing maximum polarisation amplitude in favor of faster transfer rates to compete with the rapid exchange.

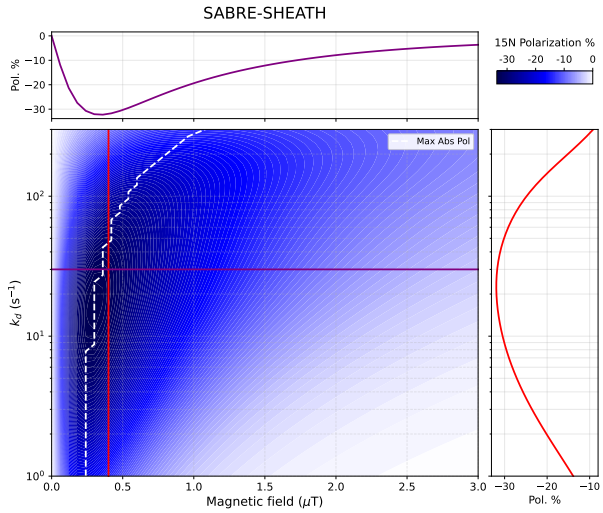

Figure S7. Simulated ^{15}N SABRE-SHEATH polarisation efficiency. The main central panel displays a 2D contour map of the final ^{15}N polarisation as a function of the external magnetic field (μT) and the chemical exchange rate k_{d} (s^{-1}, presented on a logarithmic scale). The *white dashed line* traces the magnetic field value yielding the maximum absolute polarisation for each exchange rate. The color scale indicates negative polarisation, with darker blue regions representing higher absolute transfer efficiencies (approaching -30%). The top panel presents a 1D horizontal cross-section illustrating the magnetic field dependence at a fixed optimal exchange rate of $k_{\mathrm{d}} = 30\ \mathrm{s}^{-1}$, corresponding to the solid purple line in the 2D map. The right panel presents a 1D vertical cross-section detailing the exchange rate dependence at a fixed matching field of 0.4 μT, denoted by the solid red line.

2.2 *SLIC*

The simulation results for SABRE-SLIC are shown in Figure S8. In the slow-to-intermediate exchange regime, the optimal B_1 values lie between 10 and 20 Hz. This coincides well with our experimental data, see Table 2, where all investigated compounds exhibited an optimal amplitude near 16 Hz, despite the expectation that Metronidazole (with the largest k_{d}) might require a higher value. Interestingly, the optimal B_1 experiences a sharp increase beyond $k_d \approx 90\ \mathrm{s}^{-1}$. The reason it is happening is exactly identical to the case of B_0 variation in the SABRE-SHEATH.

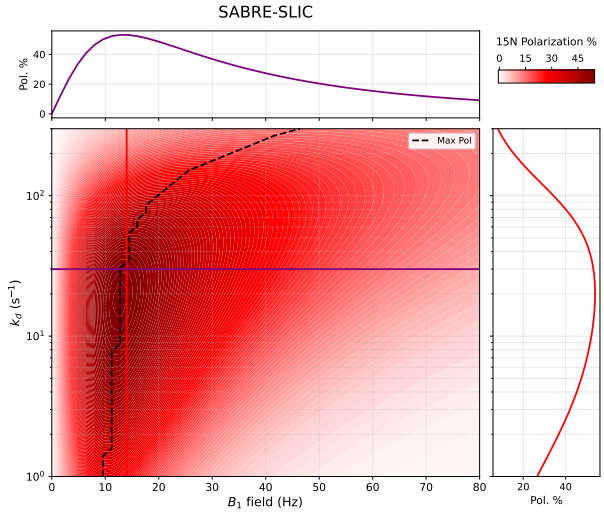

Figure S8. Simulated ^{15}N SABRE-SLIC polarisation efficiency. The main central panel displays a 2D contour map of the final ^{15}N polarisation percentage as a function of the applied continuous-wave RF field amplitude (B_1, Hz) and the chemical exchange rate k_d (s^{-1}, presented on a logarithmic scale). The color scale indicates positive polarisation, with darker red regions representing higher transfer efficiencies (approaching 50%). The black dashed line traces the optimal RF amplitude (B_1) required to maximise polarisation for each specific exchange rate. The top panel presents a 1D horizontal cross-section illustrating the B_1 field dependence at a fixed optimal exchange rate of $k_d \approx 30\ \mathrm{s}^{-1}$, corresponding to the solid purple line in the 2D map. The right panel presents a 1D vertical cross-section detailing the exchange rate dependence at a fixed matching RF field of $B_1 \approx 21$ Hz, denoted by the solid red line.

The introduction of an RF offset does not yield a global increase in polarisation, as demonstrated in Figure S9. An enhancement in transfer efficiency is observed only in the low B_1 regime, likely due to the realignment of the Level Anti-Crossing (LAC) condition. A detailed theoretical analysis of off-resonant SLIC is provided in the main text, which is consistent with previously reported results[2]. To address the limitations of the standard sequence, we propose the DRF-SLIC pulse sequence, which is detailed in the following section.

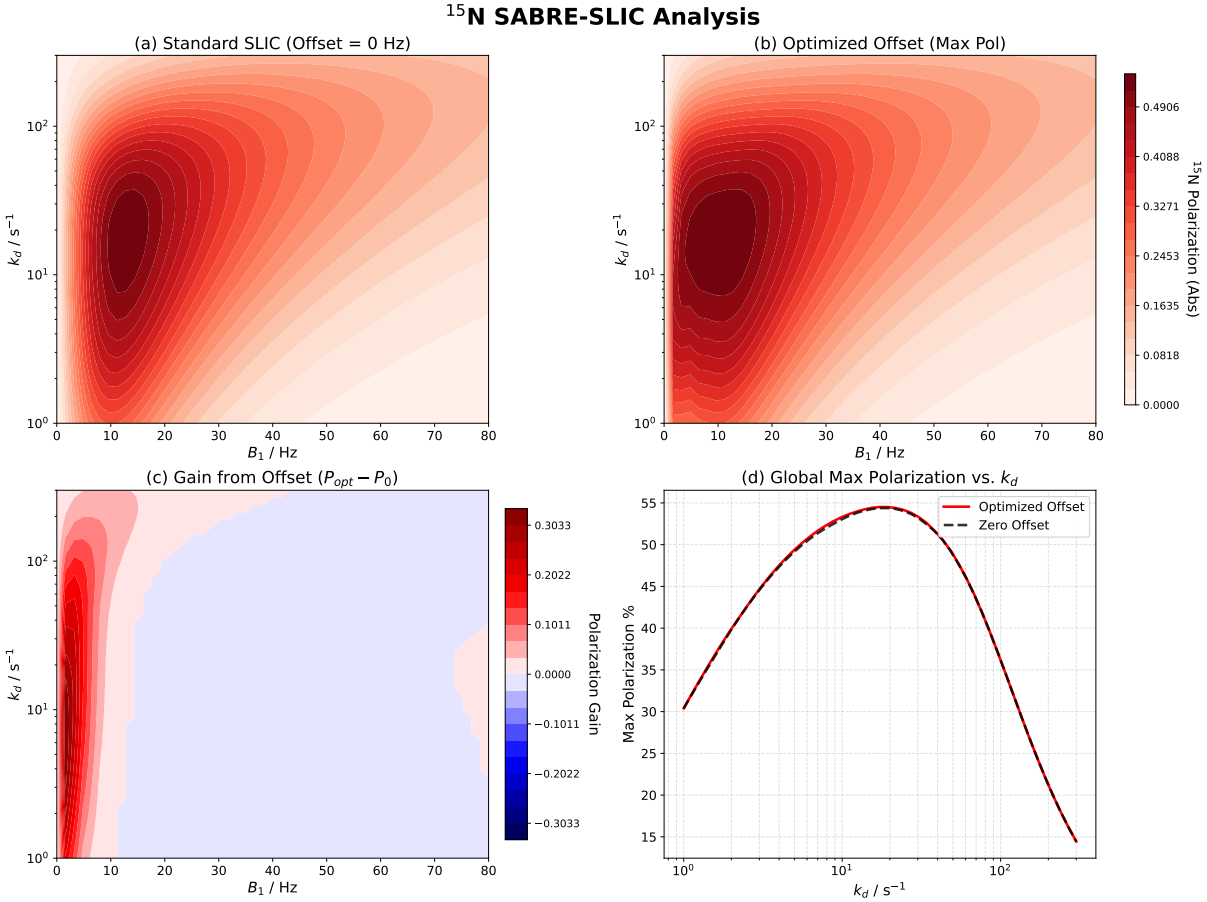

Figure S9. Impact of RF offset frequency on SABRE-SLIC performance. (a) Simulated ^{15}N polarisation map for standard SLIC (zero offset). (b) Polarisation map obtained by optimising the RF offset frequency at each (B_1, k_d) coordinate. (c) The difference map $(|P_\mathrm{opt}| - |P_\mathrm{zero}|)$, showing negligible gains across the relevant parameter space. (d) Maximum achievable polarisation as a function of the exchange rate k_d. The close overlap between the optimized (solid red) and zero-offset (dashed black) curves confirms that adding an offset does not significantly improve transfer efficiency in the SLIC regime.

2.3 *DRF-SLIC*

Since the DRF-SLIC method relies on three independent control parameters, experimentally mapping the entire parameter space would be time-consuming. However, the optimisation scans in Figure S10 reveal a convenient optimisation strategy. The optimal nitrogen nutation field ($B_{1\mathrm{N}}$) remains confined to a narrow, predictable window between 10 and 20 Hz, regardless of the exchange rate. Conversely, the nitrogen offset (Δ_N) and proton nutation field ($B_{1\mathrm{H}}$) show a broad efficiency plateau; any values exceeding 30 Hz yield an increase in polarisation, with efficiency growing slowly but steadily as the fields increase. This suggests that experimental optimisation can be simplified by fixing $B_{1\mathrm{N}}$ near 15 Hz and focusing solely on maximising the remaining two parameters.

It seems like it is generally easy to fix two of the parameters from the good value area, taking the value for the second one based on the LAC conditions, and then varying leftover on to get the final polarisation. The comprehensive 2D

heatmaps with one parameter fixed and two others being varied is shown in Figure S11. It is worth noting that the maximal polarisation along LAC lines (dashed line on the figure) is held really well for small values of k_{d}, but become not so strong at larger k_{d} values, where the requirements for faster evolution may become more important than full population transfer.

The experimental results (see Table 3) are consistent with the simulations. For a fixed $B_{1\mathrm{H}}$, the optimal $B_{1\mathrm{N}}$ lies in the range of 10–20 Hz for compounds with intermediate exchange rates (experimentally 16 Hz for acetonitrile and pyridine) and increases for compounds with faster exchange rates (30 Hz for metronidazole).Furthermore, the optimal offset frequency generally follows the Level Anti-Crossing (LAC) condition for the intermediate exchange regime, where $\nu_{\mathrm{eff}}^{\mathrm{N}} \approx \nu_1^{\mathrm{H}} \pm J_{\mathrm{HH}}$. For acetonitrile and pyridine, the experimental offset of 64 Hz aligns well with the theoretical prediction of 70 Hz. In contrast, for metronidazole, the experimental offset of 104 Hz deviates from the theoretical LAC value of 82 Hz, likely because the fast exchange dynamics disrupt the standard LAC condition.

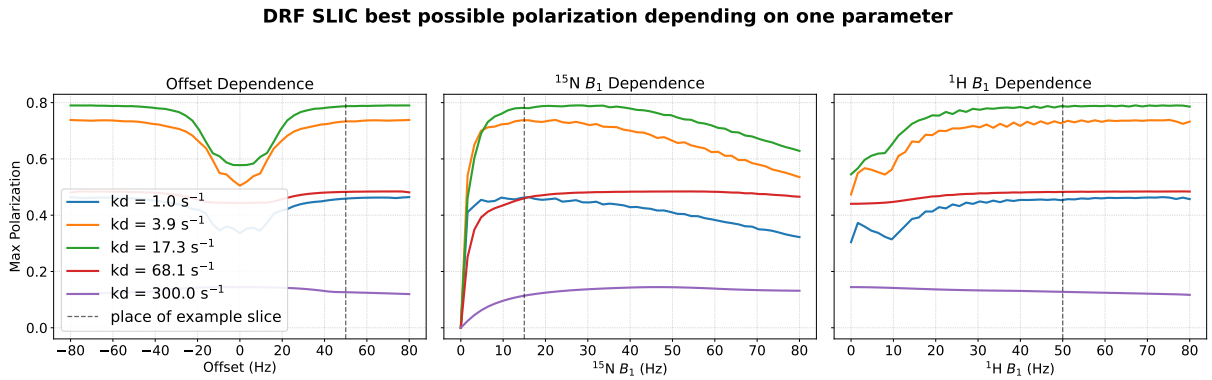

Figure S10. The panels display the maximum simulated ^{15}N polarisation as a function of a single control variable. The dependence is shown for *left* the resonance offset Δ_N, *center* the nitrogen RF amplitude B_{1N}, and *right* the proton RF amplitude B_{1H}. The colored curves represent different chemical exchange rates (k_d) ranging from slow (1.0 s^{-1}) to fast (300.0 s^{-1}) exchange. Vertical dashed lines indicate the parameter set (Δ_N = 50 Hz, B_{1N} = 15 Hz, B_{1H} = 50 Hz) selected for 2D analysis. The data indicate that while B_{1N} requires precise calibration (10-20 Hz), the Δ_N and B_{1H} parameters exhibit broad tolerance, simplifying the experimental search space.

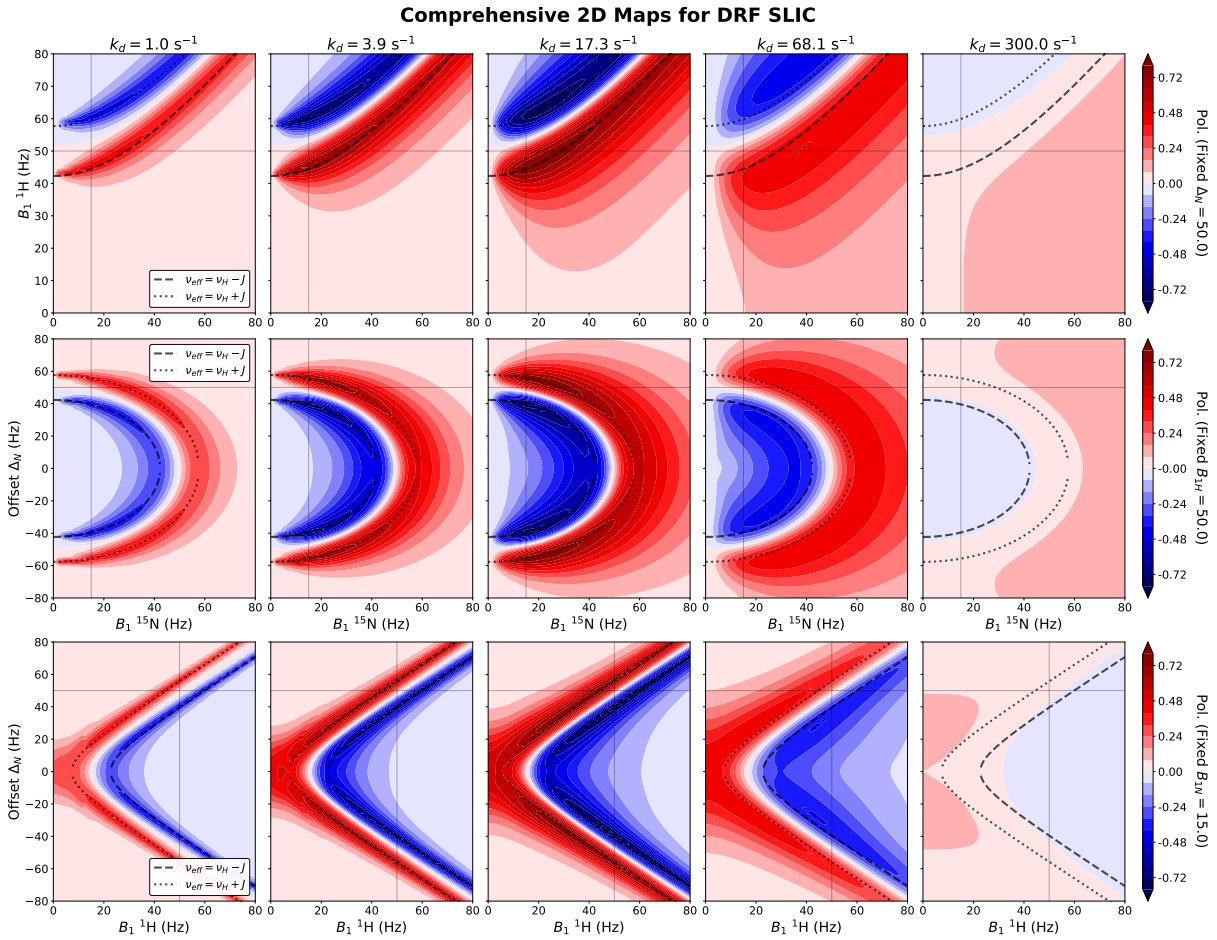

Figure S11. Simulated 2D maps of ^{15}N polarisation transfer efficiency under DRF-SLIC conditions. The contour plots display the final ^{15}N polarisation as a function of RF field amplitudes (B_{1H}, B_{1N}) and resonance offset (Δ_N). The rows present different 2D cross-sections through the parameter space by fixing one variable: (Top Row) fixed offset $\Delta_N = 50$ Hz; (Middle Row) fixed proton RF field $B_{1H} = 50$ Hz; (Bottom Row) fixed nitrogen RF field $B_{1N} = 15$ Hz. The columns correspond to increasing chemical exchange rates k_d, from 1.0 s^{-1} (left) to 300.0 s^{-1} (right). The color scale indicates signed polarisation, where red is positive and blue is negative. The overlaid black dashed and dotted curves represent the theoretical Level Anti-Crossing (LAC) conditions ($\nu_{\text{eff}}^N = \nu_{\text{nut}}^H \pm J_{HH}$), predicting the regions of maximal transfer. Thin gray solid lines indicate the fixed parameter values used in the complementary rows. The plots highlight the broadening of the efficient transfer condition as the exchange rate increases.

2.4 *PulsePol*

The resonance condition for the PulsePol sequence is defined as:

$$\tau_{\text{PP}} = \frac{2N \pm \varphi/\pi}{J} \qquad \textbf{Equation } 1.$$

Where n is the resonance number, J corresponds to the scalar coupling $J_{\text{HH}'}$, and φ is the phase shift of the second PulsePol block in radians. The effective coupling strength (dJ_*) that drives the polarisation evolution scales by a factor α, which depends on the pulse parameters:

$$dJ_* = dJ \cdot \alpha, \quad \text{where} \quad \alpha = \frac{\sin^2\left((2n\ 2\pi \pm 2\varphi)/8\right)}{(2n\ 2\pi \pm 2\varphi)/8} \text{ or } \frac{\sin^2\left(\pi J \tau_{\text{PP}}/4\right)}{\pi J \tau_{\text{PP}}/4} \qquad \textbf{Equation } 2.$$

theoretically, the most efficient coupling corresponds to the $n = 1_-$ resonance condition, which yields a scaling factor

of $\alpha_{1-}(\varphi = \pi/2) \approx 0.725$. However, in our SABRE system, this condition results in a PulsePol cycle duration that is too long relative to the ligand exchange lifetime, effectively damping the coherent transfer dynamics. Consequently, we utilise the faster $n = 0$ resonance, despite its lower theoretical scaling factor ($\alpha_{0+}(\varphi = \pi/2) \approx 0.373$).

As shown in Figure S12(a), the optimal transfer time τ_{opt} initially increases with the exchange rate k_{d}, consistent with the optimal matching condition $k_{\mathrm{d}} \approx 2\pi d J_*$. However, at higher exchange rates, the optimal duration begins to decrease. This likely occurs because the exchange lifetime $1/k_{\mathrm{d}}$ becomes comparable to the PulsePol cycle length, forcing the system toward shorter cycles to preserve coherence.

Nevertheless, significant polarisation gains are achievable in the high-k_{d} regime by deviating from the standard coherent condition, as seen in Figure S12(b, c). To maximise transfer in this regime, the phase shift must be increased beyond the theoretical prediction, as illustrated in Figure S12(d). This deviation suggests that the resonance condition can be further optimised locally, for instance, by iteratively tuning ϕ and τ around the theoretical maximum to better account for exchange dynamics (see Figure S13).

Our simulations predict an optimal pulse duration τ_{PP} in the range of 15-25 ms, which is consistent with experimentally observed resonance conditions, see Table 4. Furthermore, the model indicates that the optimal phase depends strongly on the exchange dynamics, shifting from approximately -36° for slowly exchanging species (e.g., acetonitrile and pyridine) to -72° for rapidly exchanging substrates (e.g., metronidazole).

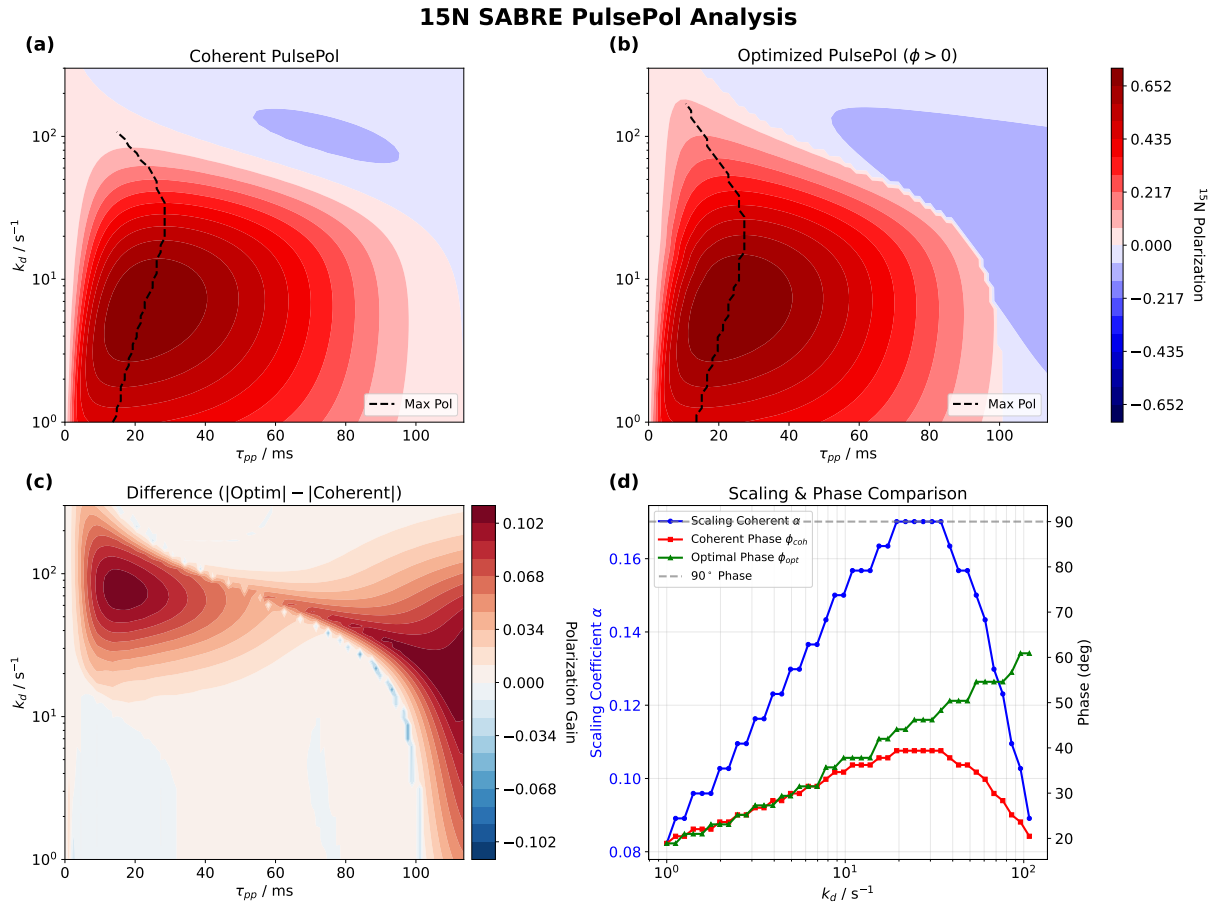

Figure S12. Comprehensive analysis of ^{15}N SABRE PulsePol performance and resonance characteristics.(a) Coherent PulsePol: Simulated ^{15}N polarisation as a function of the pulse block duration τ_{pp} and ligand exchange rate k_{d}. The pulse phase ϕ is strictly coupled to τ_{pp} via the theoretical resonance condition $\phi = \pi J \tau_{pp}$ (for the $n = 0$ resonance condition). The *black dashed line* traces the trajectory of maximum polarisation (τ_{opt}) for each exchange rate.(b) Optimized PulsePol: The maximum polarisation achievable by numerically optimizing the phase ϕ (constrained to $\phi > 0$) at each $(\tau_{pp}, k_{\mathrm{d}})$ coordinate. This represents the theoretical performance limit when the phase is tuned freely.(c) Polarisation Gain: The difference in absolute polarisation magnitude ($|P_{\mathrm{opt}}| - |P_{\mathrm{coh}}|$). Red regions indicate regimes where numerical optimization yields a higher signal than the standard theoretical condition, typically compensating for exchange-induced effects.(d) Scaling and Phase Analysis: A dual-axis comparison of parameters extracted along the maximum polarisation trajectory (dashed lines in a and b).Left Axis (Blue): The theoretical scaling coefficient $\alpha = \sin^2(\pi J \tau_{opt}/4)/(\pi J \tau_{opt}/4)$, calculated using the phase from the coherent condition. This quantifies the theoretical amplitude penalty as the optimal pulse duration increases. Right Axis: A comparison between the theoretical Coherent Phase ϕ_{coh} (red squares) and the numerically Optimal Phase ϕ_{opt} (green triangles). The divergence of ϕ_{opt} from ϕ_{coh} at higher k_{d} illustrates where the system drifts from the ideal resonance condition. The dashed gray line marks $\phi = 90°$.

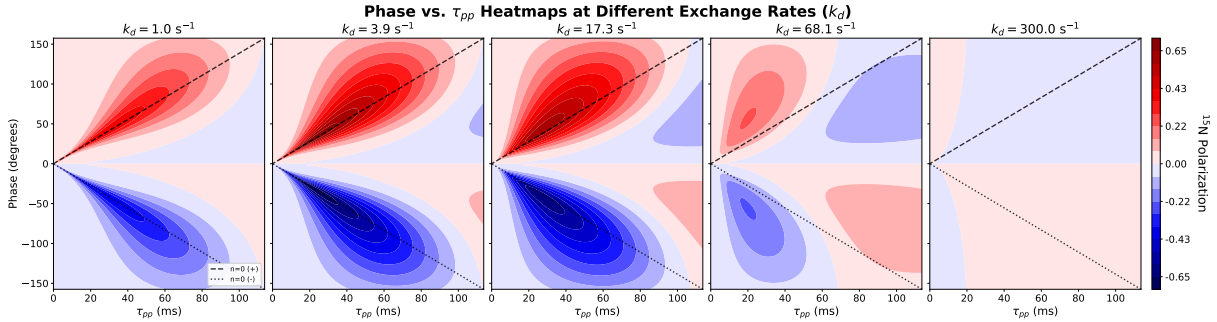

Figure S13. Phase dependence of ^{15}N polarisation at varying ligand exchange rates. Simulated ^{15}N polarisation heatmaps as a function of pulse sequence duration τ_{pp} and phase ϕ, plotted for five increasing exchange rates (k_d). As k_d increases from 1.0 s^{-1} to 300 s^{-1}, the resonance condition (visible as high-intensity red/blue bands) broadens and shifts. The black dashed lines represent the theoretical resonance condition for the $n = 0$ harmonic, derived from the coherent evolution formula $\tau_{pp} = \pm\phi/(\pi J)$. The close alignment between the simulated high-polarisation regions and these analytic lines confirms that the coherent transfer mechanism dominates, particularly at lower exchange rates. At higher k_d, the resonance features become more diffuse, indicating the interplay between coherent evolution and exchange dynamics.

2.5 *Overall comparison and coherent dynamics*

Figure S14 presents an overall comparison of the maximum achievable polarisation across different methods. Supplementing the main text, the coherent evolution using optimal SABRE parameters is shown below for various k_d values. It is evident that DRF-SLIC and PulsePol outperform SLIC and SHEATH primarily due to their ability to adjust the evolution frequency which decreases with lower k_d values while maintaining maximal transfer amplitude.

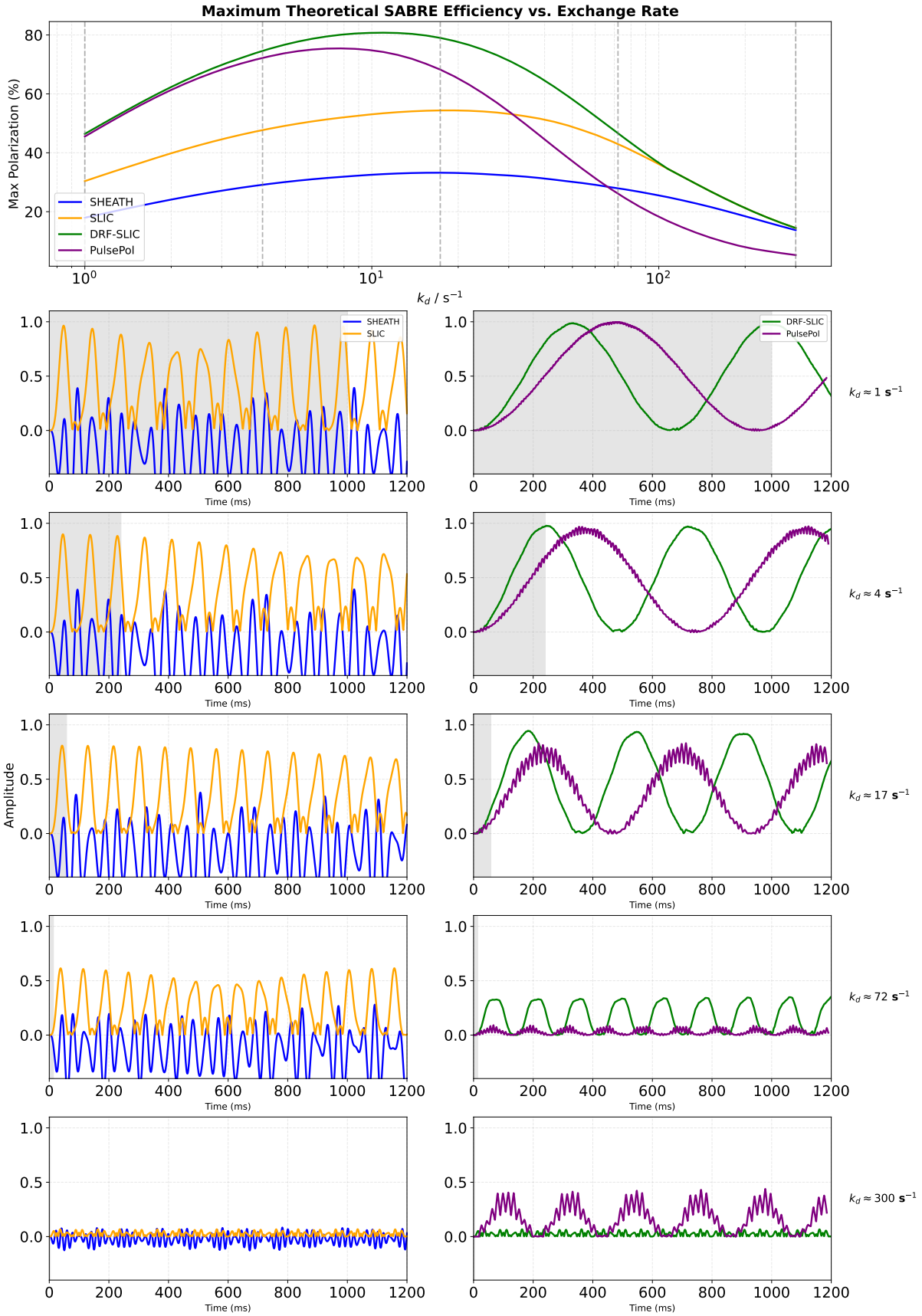

Figure S14. Theoretical limits and coherent evolution of SABRE methods. (Top) Maximum ^{15}N polarisation vs. ligand exchange rate (k_d) for SABRE-SHEATH (blue), SLIC (orange), DRF-SLIC (green), and PulsePol (purple). Vertical dashed lines indicate the five specific k_d values analyzed in the panels below. (Bottom) Time-dependent polarisation buildup for the selected exchange rates (rows). The left column compares SHEATH and SLIC methods, while the right column compares DRF-SLIC and PulsePol methods, proposed in this article. The grey shaded region represents the complex lifetime ($t \leq 1/k_\mathrm{d}$). All simulations employ optimised control parameters.

REFERENCES

1. S. Knecht, D. A. Barskiy, G. Buntkowsky and K. L. Ivanov, *The Journal of Chemical Physics*, 2020, **153**, 164106.

2. V. P. Kozinenko, A. S. Kiryutin and A. V. Yurkovskaya, *Chemistry–Methods*, 2025, **5**, e202400060.